Stopping of Swift Ions:
Solved and Unsolved Problems

Peter Sigmund*

Department of Physics and Chemistry
University of Southern Denmark
DK-5230 Odense M, Denmark

Abstract

Despite intense research in penetration of charged particles over almost a century, several central problems remain unsolved. In this paper I am trying to point out recent solutions to problem areas of long standing and, at the same time, identify specific needs from important application areas where new ideas and an increased effort are desirable. For more tutorial introductions the reader is referred to two recent monographs (Sigmund, 2004, 2006).

## Contents

* E-mail: sigmund@ifk.sdu.dk

1. General Considerations

1.1. Particle Penetration: Standard Description

Figure 1 shows a cloud chamber photograph of the slowing down of alpha particles in air. Implicitly or explicitly, many of us have such a situation in mind when addressing penetration of swift charged particles.[1] Characteristic features are almost straight trajectories of fairly uniform length, i.e., negligible multiple scattering and straggling, dependent on the accuracy aimed at. The key quantity in such a description, the continuum-slowing-down approximation, is the energy loss per travelled pathlength, usually called stopping power although stopping force is more precise, from which the total range can be determined by integration.

As a first step of a more sophisticated description, one may take into account multiple scattering and straggling in the Gaussian approximation, both being treated as minor perturbations. Such a description is employed routinely in ion beam analysis at low and intermediate resolution as well as in particle therapy (Jäkel, 2006). Conversely, such a description is insufficient in high-resolution ion beam analysis, as documented by Grande et al. (2006) and, more generally, in the study of energy transfer in thin layers or small volumes (microdosimetry).

---

[1] In accordance with common nomenclature, the term "swift" denotes projectile speeds above the Bohr velocity $v_0 = c/137$.
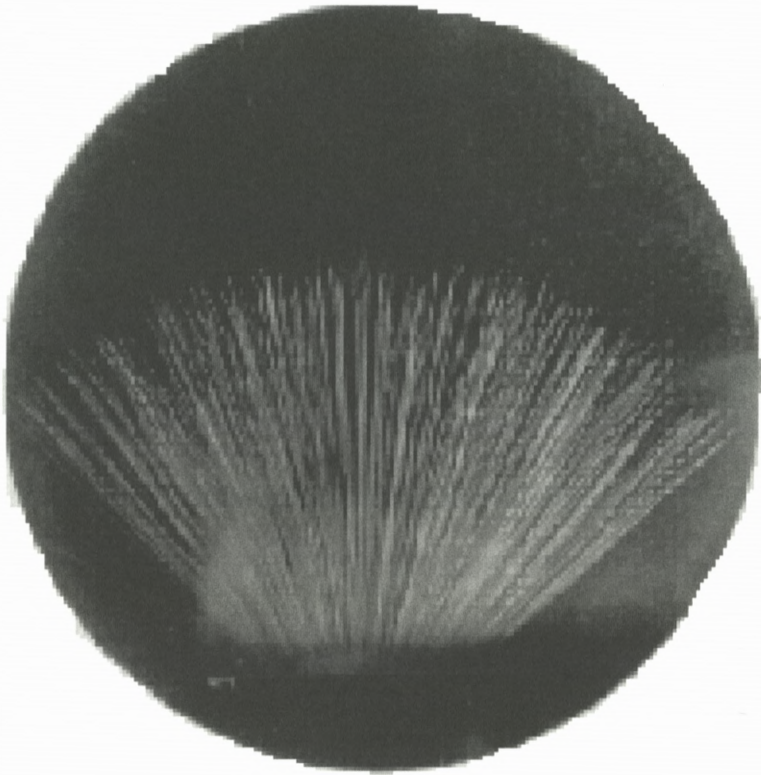
Figure 1. Cloud chamber photograph of the slowing down of alpha particles in air. From Meitner and Freitag (1926).

The model is well known to break down in case of electron and positron penetration, not the least because of excessive angular scattering, but even in light-ion penetration at low beam velocities, angular scattering is known to be a major disturbance (Schiøtt, 1966). Further complications arise in the presence of charge exchange and/or nuclear stopping.

1.2. Energy Loss, Energy Deposition and Related Quantities

Energy *lost* by the beam is the quantity of interest in ion beam analysis, but in numerous other application areas, the quantity needed is the energy *deposited* by the beam. Typical stopping measurements address energy loss, even though some of the most precise stopping data are based on measurement of deposited energy (Andersen et al., 1966).

The difference between energy loss and energy deposition is worthwhile to keep in mind, partly because energy deposition may involve energy transport by secondary particles, especially by secondary electrons but, occasionally, also by recoil atoms (Holmén et al., 1979). Serious conceptional problems may arise when potential energy becomes important, as is the case for secondary electron emission at low beam velocities (Winter et al., 2006) and, more generally, for bombardment with highly charged ions. Clearly, it does not make sense to describe the energy deposition by a slow highly charged ion in terms of an energy loss per pathlength when the travelled pathlength is essentially zero. Failure to realize this leads to misconceptions such as negative stopping powers of keV ions (Cabrera-Trujillo et al., 2002).

The prototype of an energy-loss profile is the so-called Bragg curve which, in the simplest case, is a plot of stopping force *versus* penetration depth, possibly corrected for Gaussian straggling. More appropriate for applications is a plot of the number of ionization events per travelled pathlength. This would be of interest, for example, in a detailed analysis of the particle tracks shown in Figure 1. You may be inclined to take the two quantities as proportional to each other. After all, the number of ions ν generated by a primary particle of energy E is most often estimated as $\nu = E/W$, where the "W-value" is, by and large, a constant characteristic of the stopping medium.

Figure 2 shows the stopping cross section

$$S = \sum_j \left(\int_0^{T_{\max}} T \, d\sigma(T) \right)_j \tag{1}$$

and the *ionization stopping cross section*

$$S_{\text{ioniz}} = \sum_j \left(\int_{U_j}^{T_{\max}} T \, d\sigma(T) \right)_j \tag{2}$$

for argon in silicon, where $d\sigma(T)$ indicates the cross section for energy transfer (T, dT) in a single collision event, j is a label for the silicon subshells involved and U_j the subshell binding energy. Calculations are performed by the PASS code based on binary stopping theory (Sigmund and Schinner, 2000) with input data from ICRU (2005).

Evidently, the two curves are not proportional. The ratio S_{ioniz}/S comes close to 1 somewhat below the stopping maximum. While the dropoff at low velocities due to threshold effects may be expected, a more pronounced dropoff at high speed may seem surprising. It reflects the relative significance of very soft collisions – or a large interaction volume – at high projectile speed. In order to demonstrate that
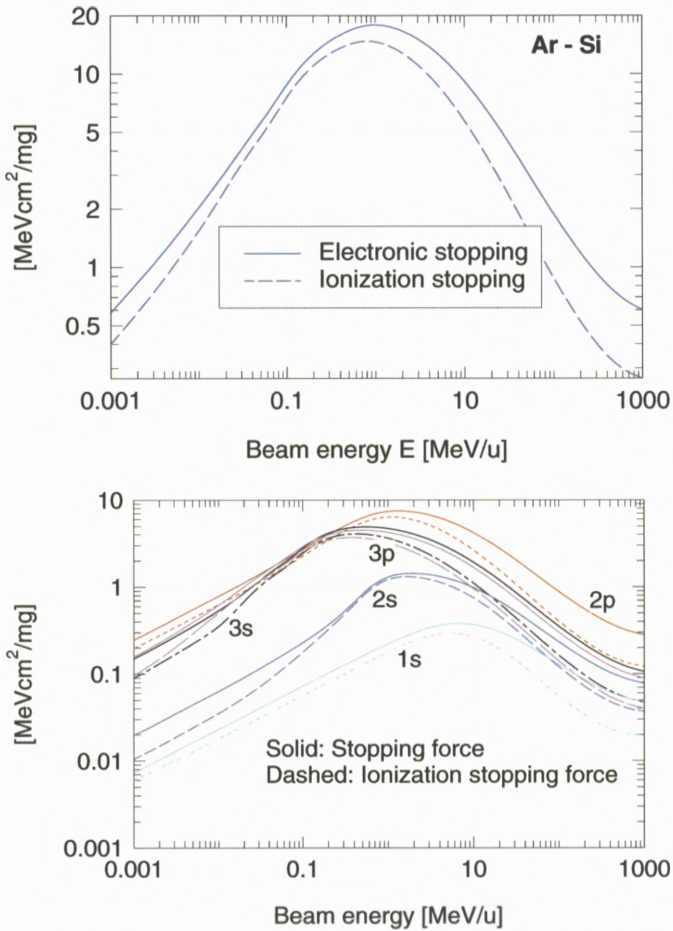
Figure 2. Stopping force on argon in silicon (solid lines) calculated from binary theory. Only target excitations considered. Dashed lines: Only energy losses exceeding the subshell binding energy included. Upper graph: All shells; lower graph: contributions from individual subshells.

this feature is unrelated to the magnitude of the shell binding energy, the lower graph shows the same information but split up into contributions from the five subshells of silicon. This feature appears important for dose planning in hadron therapy.

While energy-loss measurements typically offer less challenge to experimentalists than measurements of energy deposition, optimistic estimates of experimental error seem to be the rule rather than the exception. Figure 3 shows a typical graph of stopping data compiled by Paul (2005). Data for oxygen in gold
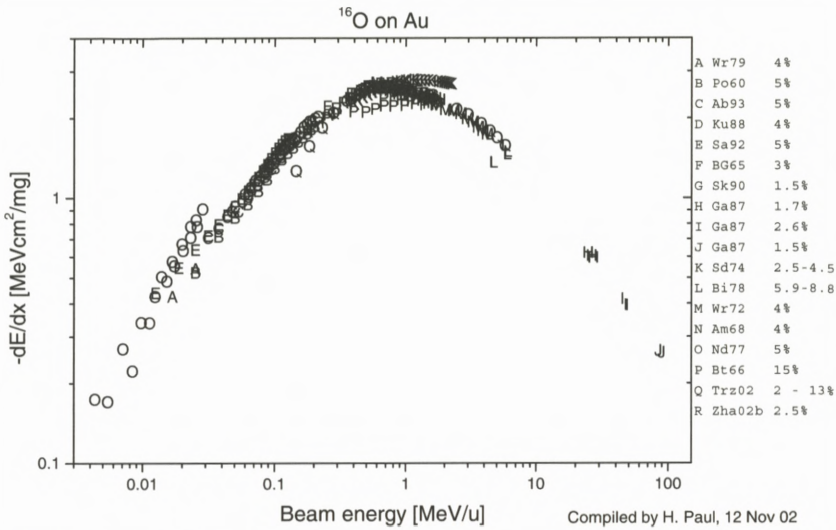
Figure 3. Measured stopping forces on oxygen in gold from numerous sources compiled by Paul (2005). Numbers on the right margin show experimental errors assigned by the respective authors.

are shown from 18 different sources. Experimental errors given in the margin are supposed to be a few per cent, while discrepancies of 20–30% between different sources are evident not only at low projectile speed but also around the Bragg peak.

2. Stopping: High and Intermediate Speed

2.1. STOPPING OF POINT CHARGES

2.1.1. *Bohr and Bethe Theory*
The stopping cross section for a point charge is conventionally written in the form[2]

$$S = \frac{4\pi Z_1^2 Z_2 e^4}{mv^2}\, L,$$ (3)

where the stopping number L reads

$$L = \begin{cases} \ln \dfrac{2mv^2}{I} & \text{(Bethe)} \\[2ex] \ln \dfrac{Cmv^3}{Z_1 e^2 \omega} & \text{(Bohr)} \quad \omega = I/\hbar \end{cases}$$ (4)

---

[2] Gaussian units are employed throughout this paper.

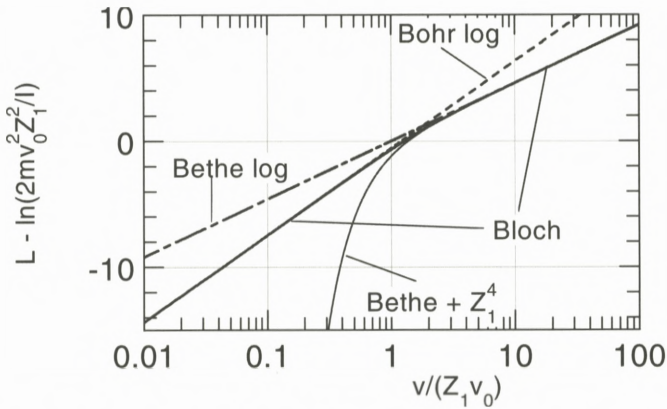*Figure 4.* The stopping number according to Bloch (1933) (solid line) approaches the Bohr and Bethe logarithms at low and high projectile speed, respectively. Also included is a curve consisting of the Bethe logarithm and the Z_1^4 correction which often, erroneously, is called the Bloch correction. $v_0 = c/137$ is the Bohr velocity. From Sigmund (1997).

in the simplest versions of Bethe and Bohr stopping theory, rerspectively. Figure 4 shows the two expressions in a plot which, within the range of validity of the two schemes, is universally valid for all point charges Z_1 and all elemental materials with atomic number Z_2.

According to Bohr (1948), the classical expression L_{Bohr} applies to the regime $\kappa = 2Z_1 e^2/\hbar v > 1$, while L_{Bethe}, based on the Born approximation, has a complementary range of validity specified by $\kappa/2 = Z_1 e^2/\hbar v < 1$. The curve labelled "Bloch" combines the two limits, the transition between which is seen to be rather abrupt. Also shown is a curve labeled "Bethe + Z_1^4", which approximates the Bloch curve in the region of small deviations from the Bethe logarithm, but which leads to absurd results at lower projectile speeds. The Z_1^4 term is often erroneously called Bloch correction.

The central empirical parameter entering both Bethe's and Bohr's expression for the stopping number is the I-value, the mean logarithmic excitation energy or, equivalently, the effective resonant frequency $\omega = I/\hbar$. There are, roughly spoken, four ways available to determine I-values:

- The local-plasma model proposed by Lindhard and Scharff (1953), where a logarithmic average of the plasma frequency is taken over the density profile of the target atom. The latter may be described either by the Thomas–Fermi model (Bonderup, 1967) or by atomic charge distributions (Chu and Powers, 1972).
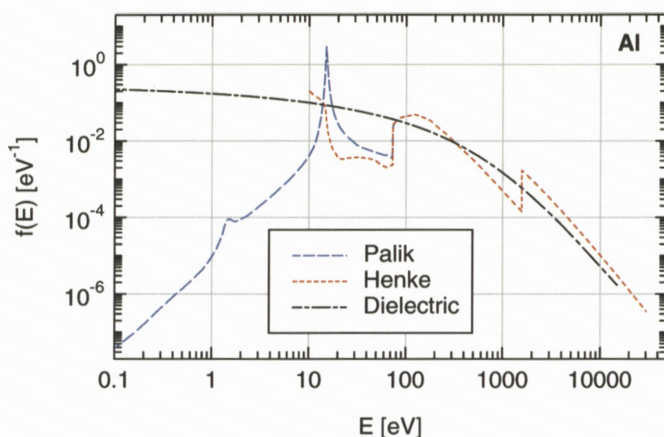
Figure 5. Oscillator-strength spectrum for metallic aluminium according to Palik (2000) and Henke et al. (1993). Also included is a curve found from the local-plasma model on the basis of the Thomas–Fermi function of a neutral aluminium atom. From Sigmund (2006).

- Fitting to measured stopping cross sections. This procedure requires reliable estimates of shell and Barkas–Andersen corrections (Andersen et al., 1969b).

- Calculation from atomic wave functions (shellwise) (Dehmer et al., 1975).

- Integration of measured oscillator strengths and photoabsorption cross sections (shellwise) (ICRU, 2005).

Figure 5 shows oscillator strength spectra for metallic aluminium from available tabulations (Palik, 2000; Henke et al., 1993), compared with a spectrum underlying the local plasma approximation, evaluated on the basis of the Thomas–Fermi density profile for a neutral atom. Evidently, the latter curve cannot reproduce the shell structure, nor does it properly describe low excitations in the free electron gas. However, it does produce a feasibly smooth average above $\sim$10 eV.

Oscillator strengths calculated from Slater orbitals by Dehmer et al. (1975) have been bundled into subshell I-values and weight factors by Oddershede and Sabin (1984). Figure 6 shows K-shell I-values tabulated by Oddershede and Sabin (1984) *versus* Z, compared with a recent evaluation on the basis of tabulated oscillator-strength spectra like those shown in Figure 5. A discrepancy is observed which approaches a factor of 5 at $Z = 36$. It is seen that for $Z > 10$, the predictions of Oddershede and Sabin (1984) even fall below the K-shell binding energy.
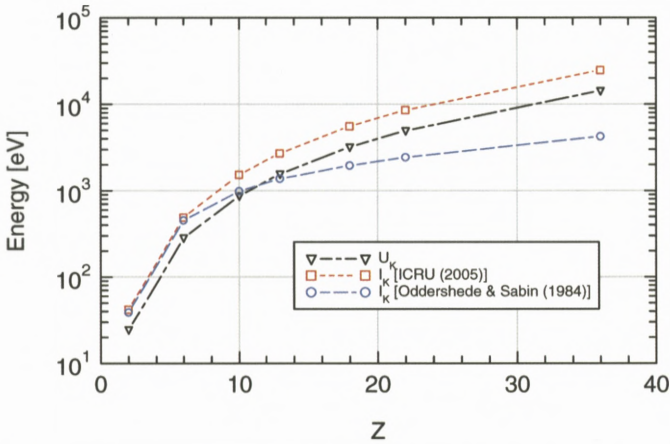
Figure 6. I-values for the K shell as a function of atomic number according to Oddershede and Sabin (1984) and ICRU (2005). Also included are K-shell binding energies. From Sigmund (2006).

2.1.2. *Additions*

The predictions of Equation (4) can only rarely stand alone but need additions. For swift point charges, such additions are conventionally classified into

1. Barkas–Andersen correction,
2. Shell correction,
3. Relativistic correction,
4. Density correction, and
5. High-Z_1 correction.

Recent progress concerns items (1), (2) and (5).

Barkas–Andersen correction   The Barkas effect denotes the difference in stopping cross section between a particle and its antiparticle. Figure 7 shows that this difference is not just a small correction $\propto Z_1^3$ to the Bethe stopping formula, as it was thought for a long time. On the contrary, it becomes exceedingly large around and below the stopping maximum. Early measurements identified a closely related effect by comparison of measured stopping cross sections for alpha particles and protons (Andersen et al., 1969a). The fact that those measurements could be described in terms of a Z_1^3 contribution suggested a very large Barkas–Andersen correction for high-Z_1 ions. However, Lindhard (1976) predicted, on the basis of a dimensional argument, a similar behavior for all projectiles in terms of the
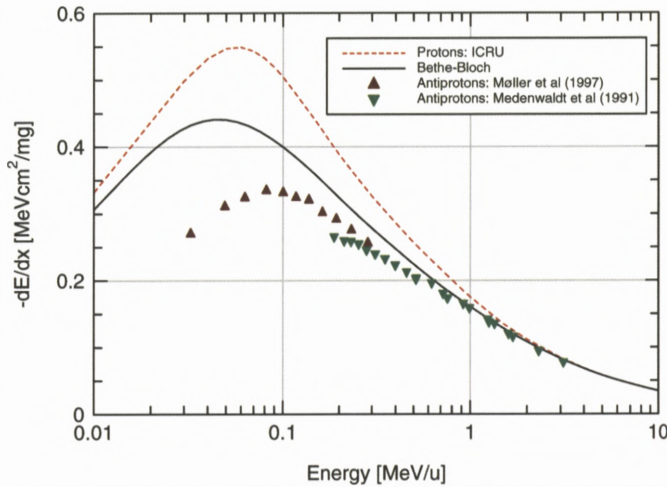
Figure 7. Barkas effect in silicon: The dotted curve represents tabulated stopping forces on protons according to ICRU (1993). Points refer to measured stopping forces on antiprotons (Medenwaldt et al., 1991; Møller et al., 1997). The solid line was found by taking the average of stopping forces calculated from binary theory for antiprotons and protons.

Bohr scaling variable $mv^3/Z_1e^2\omega$. This prediction has been confirmed in recent calculations by Sigmund and Schinner (2003).

Reliable estimates of the Barkas–Andersen corrections for protons and antiprotons on the basis of several theoretical schemes have become available in recent years, cf. ICRU (2005) or Sigmund (2006) for reviews.

A particularly controversial topic was the question of whether the Barkas–Andersen correction received contributions from distant collisions only, as asserted by Ashley et al. (1972) or, following an argument by Lindhard (1976), also from close collisions. Figure 8 shows calculations for a target atom modelled as a spherical harmonic quantum oscillator. The upper graph shows the mean energy loss *versus* impact parameter in the first Born approximation ($\propto Z_1^2$), while the lower graph shows the contribution from the second Born approximation ($\propto Z_1^3$), for a wide range of the Bethe parameter $2mv^2/\hbar\omega$. While there are quantitative differences, there is clear evidence for a contribution also from close collisions in the graph on the bottom. This behavior has been confirmed in all recent studies, with the exception of a classical-trajectory Monte Carlo simulation by Grüner et al. (2004). Possible origins of that discrepancy are still being discussed.

Shell correction   The shell correction prevents the stopping number from becoming negative at low speed, as would be the case if it were estimated from
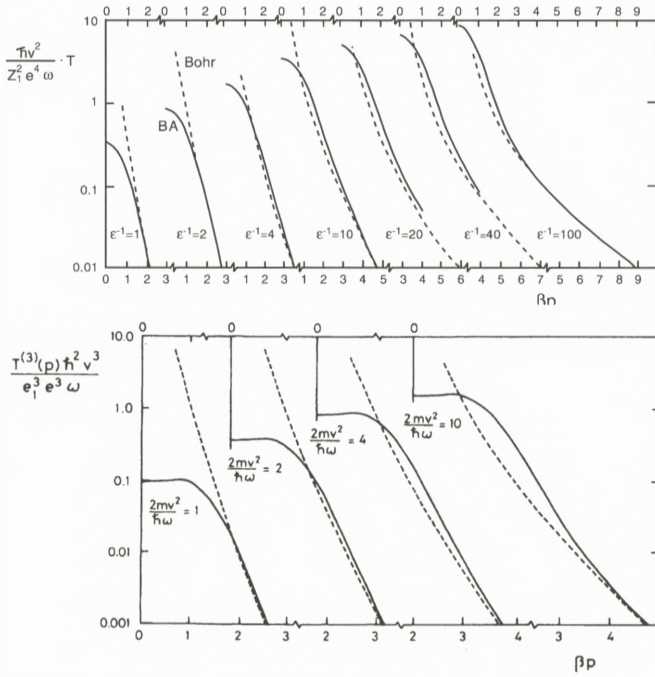
Figure 8. Energy loss in single collision *versus* impact parameter for a spherical harmonic os-
cillator. Upper graph: First Born approximation (Mikkelsen and Sigmund, 1987); lower graph:
contribution from second Born approximation (Mikkelsen and Sigmund, 1989).

the Bethe logarithm alone. Following a tradition established by Walske (1952),
this correction is evaluated separately for each principal shell of the target.
This implies that in particular for high-Z_2 materials, shell corrections may be
non-negligible even at rather high projectile speeds.

Several theoretical schemes have been proposed, and utilized successfully, for
evaluating shell corrections. For reviews see Fano (1963) and Sigmund (2006). A
point of discussion, however, has been the origin of the correction. An asymptotic
expansion for high but non-relativistic projectile speed yields $-\langle v_e^2 \rangle / v^2$ as the
leading correction in the stopping number, where v_e denotes the orbital speed of
a target electron. On this basis, the primary cause of the shell correction has been
understood to be the neglect of the orbital velocity in comparison to the beam
velocity, when the transition is made from the rigorous Born approximation to the
Bethe logarithm.

However, the Bohr formula also shows a logarithmic dependence on projectile
speed, even though the classical Bohr model operates with an initially stationary
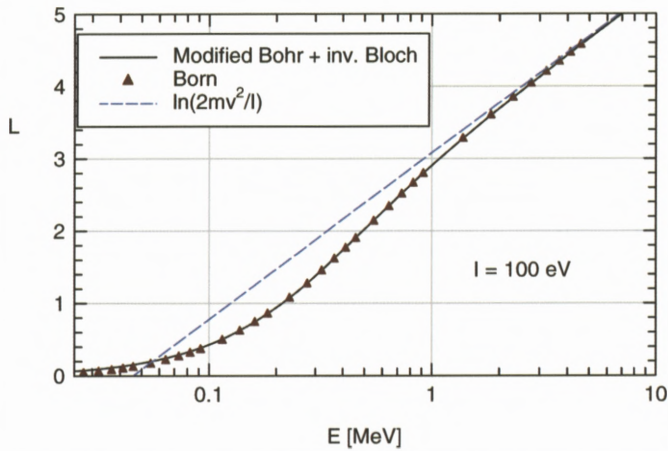
Figure 9. Stopping number of a spherical harmonic oscillator. Triangles: Born approximation for quantum oscillator (Sigmund and Haagerup, 1986). Dashed line: Bethe logarithm. Solid line: Bohr theory (logarithmic expansion avoided) plus inverse-Bloch correction. Orbital motion included via kinetic transformation (Sigmund, 1982). From Sigmund and Schinner (2006).

target electron. In that case, it is easily seen that the logarithmic dependence arises purely mathematically from an asymptotic expansion of a Bessel function, which can readily be avoided (Sigmund, 1996).

Figure 9 illustrates the situation on a target modeled as a spherical harmonic oscillator. The straight line represents the Bethe logarithm. The triangles represent the rigorous result for the Born approximation (Sigmund and Haagerup, 1986), while the solid line reflects the sum of an accurate evaluation of the Bohr stopping number – i.e. beyond the logarithmic approximation – plus the inverse-Bloch correction – which ensures that the Bethe formula is approached for $\kappa < 1$ – both terms being kinematically corrected in accordance with the velocity spectrum of the quantum oscillator.

Sigmund and Schinner (2006) concluded from the perfect agreement that the shell correction is made up by two distinct contributions: A mathematical correction that can be repaired in the classical Bohr expression, and a kinematic correction taking into account the velocity spectrum of the target atom.

Relativistic corrections within the Born approximation have been known for a long time and reviewed by Fano (1963). Corrections beyond the Born approximation were found experimentally by several groups (Tarlé and Solarz, 1978; Scheidenberger et al., 1994). Theoretical attacks go back to Ahlen (1980, 1982) and Scheidenberger et al. (1994). A powerful analysis on the basis of the
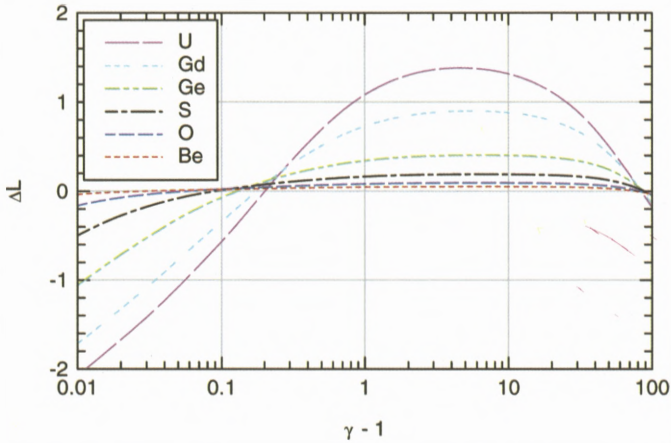
Figure 10. Correction to relativistic Bethe formula according to Lindhard and Sørensen (1996). $\gamma = 1/\sqrt{1 - v^2/c^2}$. From (Sigmund, 2006).

phase shifts for relativistic Coulomb scattering was presented by Lindhard and Sørensen (1996). This analysis does not only comprise the Mott correction and what was called the relativistic Bloch correction, but also allows for deviations from Coulomb scattering due to the non-vanishing size of the projectile nucleus. Figure 10 shows the relativistic high-Z_1 correction for several values of Z_1. While it is quite small for the lightest ions, it is very substantial for $Z_1 > 10$, once the kinetic energy of the projectile approaches or exceeds its rest energy.

2.2. STOPPING OF DRESSED IONS

For ions carrying electrons, additional effects need to be considered,

1. Screening of the Coulomb interaction by electrons accompanying the projectile,
2. Excitation amd ionization of the projectile by collisions with target atoms,
3. Energy loss by charge exchange.

While the second and third process have received comparatively little attention in the literature, the first one represents one of the most lively discussed topics in the field of particle penetration, with the central keywords being the effective ion charge and the so-called gas-solid paradox.

2.2.1. *Effective Ion Charge: A Misleading Concept*

In a first attempt to estimate the stopping of fission fragments after the discovery of uranium fission, Bohr (1940) employed his classical stopping formula but inserted an effective ion charge $q_1 e$ instead of the nuclear charge $Z_1 e$. The magnitude of q_1 was estimated from a simple adiabaticity criterion.

While this appears reasonable in the absence of a more accurate estimate, Northcliffe (1963) suggested to apply the same procedure but implying validity of the Bethe stopping cross section, with an effective charge defined by

$$q_{1,\text{eff}}^2 = Z_{1,\text{ref}}^2 \frac{S(Z_1, v)}{S(Z_{1,\text{ref}}, v)}, \tag{5}$$

where $S(Z_1, v)$ represents the stopping cross section in charge equilibrium of an ion with atomic number Z_1 as a function of speed, and $Z_{1,\text{ref}}$ a reference ion, typically a proton or an alpha particle.

Equation (5) is highly problematic in several respects,

- Screening is important for $v \lesssim Z_1^{2/3} v_0$, while Bethe theory is valid for $v > Z_1 v_0$. Thus, Bethe theory cannot be assumed to be valid in the velocity regime of substantial screening.
- A more accurate description of stopping in the screening regime would have to start at the Bohr formula which does not predict a stopping cross section $\propto Z_1^2$.
- Both Bethe's and Bohr's formulae have been derived for point projectiles. For screened-Coulomb interaction, neither formula can be taken to be valid.

In Figure 11, the solid line represents a calculated effective-charge ratio $q_{1,\text{eff}}^2 / Z_1^2$ for oxygen in amorphous carbon with helium as the reference ion. It shows a characteristic S shape with an approach toward unity at high velocities for vanishing screening, and a drop-off to almost 0.1 at low projectile speed. The experimental points in the graph – which refer to a large number of target materials – show that this behavior is also found by inserting measured stopping cross sections for both the ion of interest and the reference ion. It has almost universally been ascribed to projectile screening in the literature. However, as is seen from the dashed line in Figure 11, a similar, almost as pronounced S shape is found when calculated stopping cross sections for bare ions are inserted both for the ion of interest and the reference ion. If the effective-charge concept were valid, a constant $= 1$ would be expected. From the location of the classical limit $\kappa = 1$, we may conclude that *the effective-charge model ascribes effects to projectile screening which are actually caused by the breakdown of Bethe theory and the transition to the classical regime.*
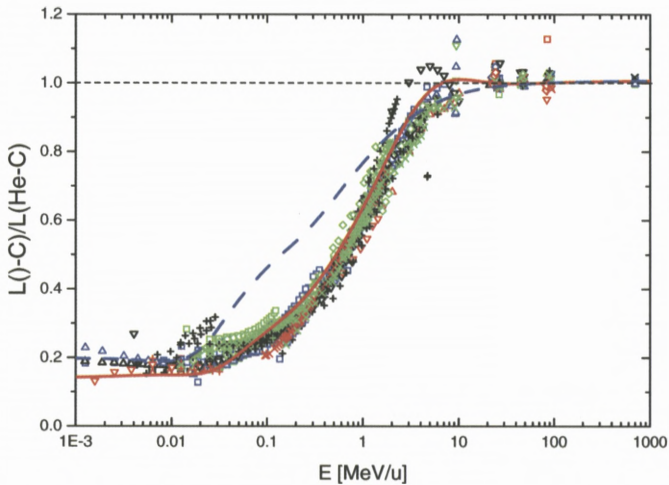
Figure 11. Stopping ratio O-C/He-C calculated from binary theory. Solid red line: Both ions in charge equilibrium. Dashed blue line: Both ions bare. From Sigmund and Schinner (2001a) and ICRU (2005). Experimental points for oxygen ions on a large number of targets according to Paul (2005).

Thus, while Equation (5), when utilized as a purely empirical relation to scale measured stopping cross sections with the aim of interpolation, may be useful at least for (Z_1, Z_2) pairs in the neighborhood of experimental data, it grossly misrepresents the physics involved, the error being up to a factor of 5 in the case depicted in Figure 11. This immediately explains why attempts to relate the effective charge to the actual ion charge were notoriously unsuccessful. Furthermore, there is no reason to expect the effective charge to exhibit Thomas–Fermi scaling behavior of the kind obeyed by the equilibrium ion charge, an assumption underlying e.g. the popular SRIM code (Ziegler, 2005).

2.2.2. *Charge-Dependent Stopping and Gas-Solid Paradox*
Several theoretical schemes have become available during the past decade to estimate stopping cross sections for dressed ions, in particular

- the convergent kinetic theory scheme by Maynard et al. (2001),
- the binary theory by Sigmund and Schinner (2000, 2002b),
- the unitary convolution approximation by Grande and Schiwietz (2002), and
- the scheme of Arista (2002) based on a generalization of the Friedel sum rule.
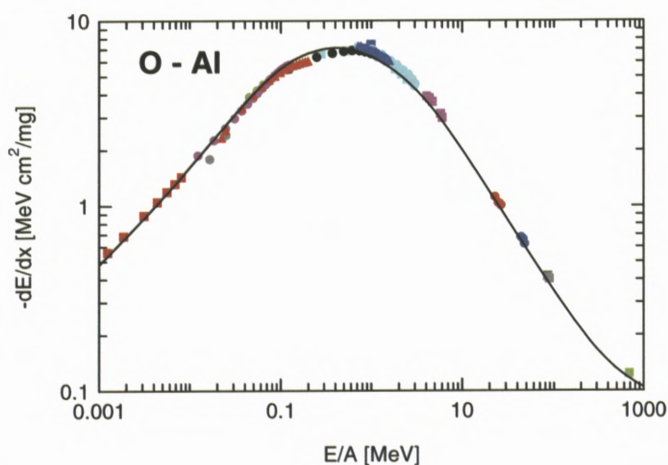
Figure 12. Stopping of oxygen in aluminium. Experimental data compiled by Paul (2005). Theoretical prediction from binary theory. From Sigmund and Schinner (2002b).

Apart from the theoretical tools applied, the schemes also differ in the way how various corrections to equivalents of the Bohr or Bethe formula are taken into account. For details the reader is referred to Sigmund (2004).

Any of the above schemes can be utilized to estimate stopping cross sections in charge equilibrium by using suitable data for mean equilibrium charges or, preferrably, equilibrium charge fractions. Figure 12 shows, as an example, a comparison of measured equilibrium stopping cross sections for oxygen in aluminium with the prediction of the binary theory.

It was found experimentally by Lassen (1951b) that equilibrium charge states of fission fragments tend to be significantly higher in solids than in gases. Moreover, for gases, a weak increase with gas pressure was found (Lassen, 1951a). An explanation of this phenomenon was presented by Bohr and Lindhard (1954) who ascribed it to short free pathlengths for electronic collisions in condensed matter, where excited projectiles would not have time to deexcite into their ground states and thus would exhibit higher ionization cross sections.

A seeming problem with this explanation was considered to be the lack of a corresponding enhancement in the measured stopping cross sections. Although such an enhancement was found subsequently (Geissel, 1982; Bimbot et al., 1989a, 1989b), it was smaller than expected. A proposed explanation of this so-called charge-state paradox was the assertion that there was no difference between charge states in solids and gases, and that the enhanced charge state in case of solids was a post-foil effect due to emission of Auger electrons (Betz and

Grodzins, 1970). That assertion, however, could not be verified, since the required number of Auger electrons was never found in pertinent experiments.

While the claim of a paradox presumably was justified until 1982, where no evidence of enhanced stopping cross sections was available, the main problem afterwards was the more or less explicit belief in the validity of a q_1^2 dependence of the stopping cross section on the ion charge. The problem evaporated, once it was recognized that the actual dependence was weaker and that even for bare ions, Bohr theory does not predict a Z_1^2 dependence because of the occurrence of Z_1 in the logarithm. For explicit discussions the reader is referred to Sigmund (1997) or Maynard et al. (2000).

2.2.3. *Projectile Excitation/Ionization; Antiscreening*

A projectile carrying bound electrons does not only lose energy by excitation of the target but also by excitation of its own electrons. As a first approximation one may treat this process as the interaction between a screened (neutral) target nucleus and a partially screened projectile. For $Z_1 = Z_2$, this process will be less important than target excitation because

- a neutral particle represents a weaker perturbation than a partially stripped one,
- there are fewer electrons to be excited on the projectile than on the target, and
- electrons on the projectile are more strongly bound in the average.

It is also clear that projectile excitation decreases in importance with increasing projectile speed because of a decreasing number of bound electrons. However, the effect must be expected to increase in importance for ions with Z_1 exceeding Z_2.

An interesting difference between atomic-collision physics and particle stopping was pointed out recently by Sigmund and Glazov (2003). In atomic-collision physics, the quantity of interest is the inelastic energy loss,

$$6Q = \epsilon_{\text{target}} + \epsilon_{\text{projectile}}, \tag{6}$$

where ϵ represents the excitation energy of the target and projectile, respectively, from their respective initial states. This relation also holds for excitation into the continuum.

In particle stopping, somewhat contradictory to common nomenclature, it is actually not the total energy loss per pathlength that defines the stopping force but the change in velocity or momentum of the projectile nucleus. This implies that Equation (6) holds for discrete excitations while for the continuum, i.e., projectile

ionization, the matter is more complex. Indeed, for screened-Coulomb interaction with the target atom, electrons are ejected from the projectile predominantly in the backward direction, seen in a reference frame moving with the ion, and hence move more slowly than the ion, seen in the laboratory frame of reference. Thus, such electrons actually give rise to an *increase* in projectile speed instead of a decrease. However, the effect is small. As a consequence, and in accordance with the conclusion of Sigmund and Glazov (2003), only projectile *excitation* is taken into account in tabulations of stopping cross sections (ICRU, 2005), while the effect of projectile ionization is simply ignored.

Stimulated by experience in atomic-collision physics, an effect called anti-screening has occasionally been discussed in connection with particle penetration (Kabachnik, 1993). It denotes the phenomenon that a projectile electron, rather than screening the charge of the projectile nucleus, may cause excitation of target electrons by electron-electron interaction, while the nuclei act as spectators. In this way, energy losses exceeding those estimated for Coulomb interaction with a bare ion may be achievable. Clearly, target excitation by such processes is intimately coupled to projectile excitation. I have presented estimates (Sigmund, 1997) indicating that the effect decreases rapidly as Z_1 becomes > 1. The effect has been ignored in all quantitative estimates of stopping cross sections to the author's knowledge. It has been considered in a recent study by Montanari et al. (2003). Those results, however, seem questionable because of the failure to recognize the essential difference between projectile excitation and ionization.

2.2.4. *Charge Exchange*

Charge exchange is known to contribute to the mean energy loss mainly below the stopping maximum, in particular for light ions (Golser and Semrad, 1991; Schiwietz, 1990). In the model of Firsov (1959) for inelastic energy losses of heavy ions, all energy transfer is assumed to be due to electron capture by the projectile from the target. A comprehensive study of the influence of charge exchange *on the stopping cross section*, in particular a specification of conditions under which the effect is negligible, would be desirable.

2.3. VALENCE STRUCTURE EFFECTS

The valence structure of the target has unquestionably an influence on atomic stopping cross sections and may produce

1. non-monotonic variations with atomic number, commonly called Z_2 structure or Z_2 oscillations,

2. atom-molecule differences, commonly denoted as deviations from Bragg additivity,
3. gas-solid differences, and
4. conductor-insulator differences.

While the first two effects are well established experimentally, little quantitative information is available regarding the latter two, not the least because it may be hard to separate them from the others, both experimentally and theoretically.

As a general rule, one may assume that valence structure effects are most pronounced for light target materials, simply because of a large fraction of valence electrons (ICRU, 1993).

Z_2 structure and deviations from Bragg additivity have commonly been analysed in terms of pertinent I-values (Chu and Powers, 1972; Thwaites, 1984; ICRU, 1993). This is justified in the range of beam velocities where these effects are small. However, the logarithmic dependence of both Bohr and Bethe stopping cross section on I suggests valence effects to increase with decreasing projectile speed. This trend is enhanced by the gradually decreasing influence of inner taget shells on the stopping cross section as the velocity decreases. A recent study (Sigmund et al., 2005) indicates that in the velocity regime of pronounced valence effects, shell and Barkas–Andersen corrections are at least as important as I-values in quantitative predictions.

In view of the absence of experimental data, predicted deviations from Bragg additivity for heavy ions have usually been determined by scaling experimental results for proton and alpha-particle bombardment (Ziegler, 2005). This assertion has not been corroborated by theory: In the velocity range where valence structure effects become significant for protons and helium ions, heavier ions are strongly screened. This implies a drastic reduction of the contribution of distant collisions to the stopping cross section, and hence much less pronounced valence structure effects. Conversely, the most pronounced effects were found in the stopping of antiprotons (Sigmund et al., 2003).

2.4. CHANNELING

Early studies of energy loss in channeling (Lindhard, 1965) were handicapped by the absence of reliable estimates of impact-parameter-dependent energy losses. Therefore, most estimates going beyond the use of the equipartition rule employed the local-plasma picture, even though this picture is much more questionable for impact-parameter-dependent energy losses than for stopping cross sections.

Several of the theoretical schemes mentioned above allow to estimate impact-parameter dependencies, in particular so the harmonic-oscillator model

(Mikkelsen and Mortensen, 1990), binary theory (Sigmund and Schinner, 2001b), and the unitary-convolution approximation (Azevedo et al., 2000). Considering the large number of available experimental data, here is a widely open area for thorough and comprehensive study.

A problem of long standing in this area is the Barkas–Andersen effect for channeled ions. In experiments with heavy ions in "frozen charge states", Datz et al. (1977) and Golovchenko et al. (1981) found energy losses strictly proportional to the square of the charge state, i.e., seemingly no Barkas–Andersen correction. We have looked into this problem (Sigmund and Schinner, 2001b) and arrived at some degree of understanding. Conversely, Azevedo et al. (2001) found what they call a giant Barkas effect for low-Z_1 ions with a maximum for channeled lithium ions. For random stopping, on the other hand, the maximal Barkas–Andersen effect was predicted to be observable for protons (Sigmund and Schinner, 2003). Some clarification is evidently needed here.

3. Straggling

The term "energy-loss straggling" is commonly used either for the variance of an energy-loss profile,

$$\Omega^2 = NxW = \left\langle (\Delta E - \langle \Delta E \rangle)^2 \right\rangle, \tag{7}$$

which is proportional to the travelled path length x and atom density N for random stopping, or for the energy-loss profile $F(\Delta E, x)\,\mathrm{d}(\Delta E)$ itself.

In principle. also higher cumulants $\langle (\Delta E - \langle \Delta E \rangle)^n \rangle$ with $n \geq 3$ are of interest, although measured results are scarce in the literature: These quantities are sensitive to the high-loss tail of the spectrum and, hence, to background noise.

Straggling is a complex topic and has been much less studied than the mean energy loss. One reason is that straggling is not the only reason for observed broadening of an energy-loss profile: Non-uniform layer thickness and target inhomogeneities may compete and sometimes become dominant, and separating these effects from straggling is by no means trivial.

This survey is rather brief. For a more comprehensive account the reader is referred to Sigmund (2006, chapters 8 and 9).

3.1. VARIANCE AND STRAGGLING PARAMETER

3.1.1. *Factors Affecting Straggling*
The generally accepted reference standard in straggling is "Bohr straggling",

$$W_\mathrm{B} = 4\pi Z_1^2 Z_2 e^4, \tag{8}$$

which represents the fluctuation of the energy loss of a point charge $Z_1 e$ penetrating through a medium filled randomly with free electrons at a density of $Z_2 N$ [electrons/volume]. Note that Bohr straggling does *not* represent the prediction of the Bohr stopping model for straggling: Binding of target electrons is neglected here.

In principle, all factors influencing the stopping cross section also affect the straggling parameter, i.e.,

- Binding,
- Orbital motion (shell correction),
- Barkas–Andersen effect,
- Projectile screening and excitation, and
- Relativity.

Lindhard and Sørensen (1996) have shown that there is no non-relativistic Bloch correction in straggling, i.e., similar predictions ought to emerge from the Born approximation on the one hand and the Bohr model on the other. However, in the same work it was demonstrated that the relativistic high-Z_1 correction is quite important also in straggling.

Moreover, charge exchange has long been known to produce drastic effects in straggling. In addition, bunching and correlation are effects which are of no significance to the mean energy loss for a uniform beam but can be substantial in straggling.

3.1.2. *Shell and Barkas–Andersen Correction*

Figure 13 shows a set of recent predictions for protons and antiprotons in silicon, split up into contributions from the principal target shells. All curves have been normalized to Bohr straggling. In addition to the curves for protons and antiprotons, also average curves are shown, i.e., results ignoring the Barkas–Andersen correction.

In the high-speed limit, Bohr straggling is approached, with the contributions from individual shells reflecting the number of electrons in those shells. A pronounced overshoot, the Bethe–Livingston shoulder, is observed at intermediate speed, in particular for protons interacting with the L-shell. This is a manifestation of the shell correction (Fano, 1963). Figure 14 shows an experimental verification of this effect.
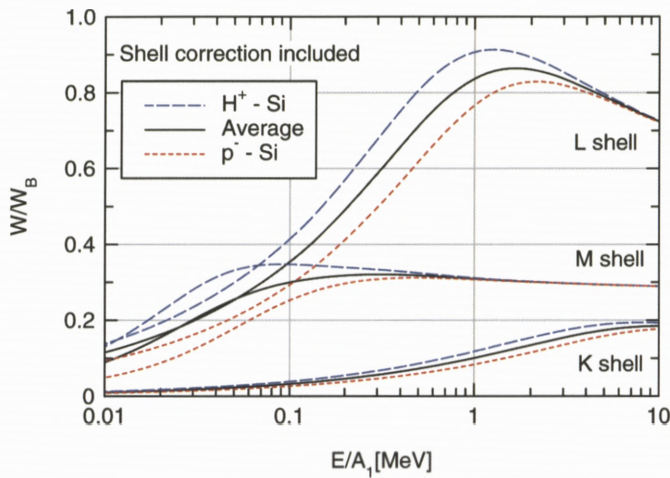
Figure 13. Straggling for protons and antiprotons in silicon predicted from binary theory, split into contributions from the principal shells. From Sigmund and Schinner (2002a).
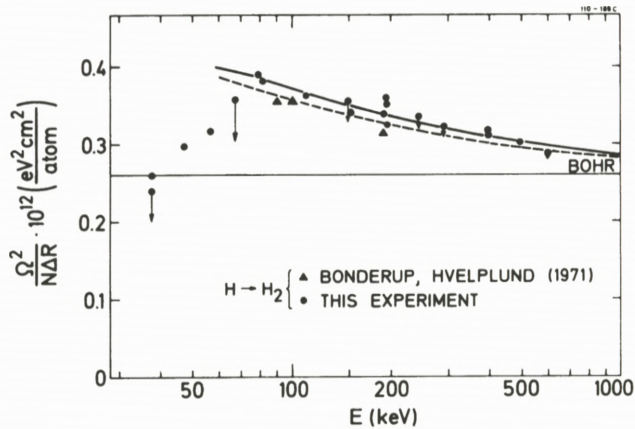
Figure 14. Straggling for protons in hydrogen. Measurements by Besenbacher et al. (1981) compared to calculations by Bonderup and Hvelplund (1971). The solid and dashed line represent two versions of the Thomas–Fermi description of the I-value. From Besenbacher et al. (1981).

3.1.3. *Bunching and Correlation*

As mentioned above, Bohr straggling assumes electrons distributed at random. Deviations from Poisson behavior occur when electrons are not distributed randomly in space.

Figure 15. Straggling of protons and helium ions in argon gas. Measurements from Besenbacher et al. (1981). Calculations from binary theory. From Sigmund and Schinner (2002a).
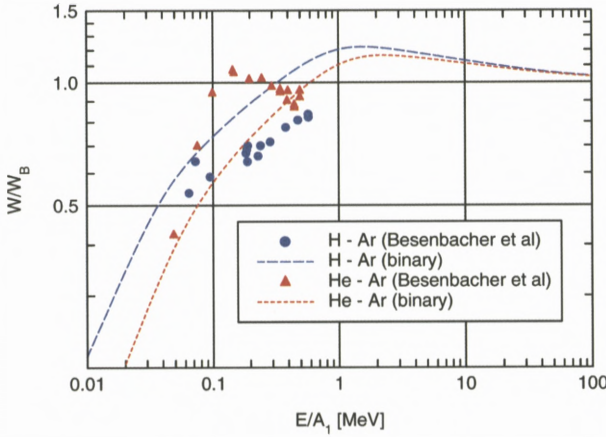
- The *bunching effect* takes into account enhanced straggling due to the proximity of electrons in a target atom.
- *Correlation*, on the other hand means

  – Enhanced straggling due to proximity of atoms in the molecules of a gas, or
  – Diminished straggling due to dense packing of atoms in (amorphous) solids (Sigmund, 1978).

Contributions of bunching and correlation to straggling go roughly with the square of the atomic stopping cross section (Sigmund, 1976, 2006; Besenbacher et al., 1980). Figure 15 shows measured straggling parameters for protons and helium ions in argon gas. It seen that due to bunching, the curve for helium shows a pronounced enhancement near the stopping maximum. Theoretical curves, calculated from binary theory, have been determined by ignoring the bunching effect.

Figure 16 demonstrates the existence of the molecular correlation effect, i.e., enhanced straggling roughly $\propto S^2$ for a molecular gas (N_2) as compared to a similar atomic gas (Ne).

Figure 17 shows measured straggling parameters for light ions in germanium. Binary theory predicts a pronounced Bethe–Livingston shoulder, which is not found experimentally. One possible explanation is the correlation effect which, in a solid, gives rise to decreased straggling (Sigmund, 1978), and which has not been included in the theoretical curves.
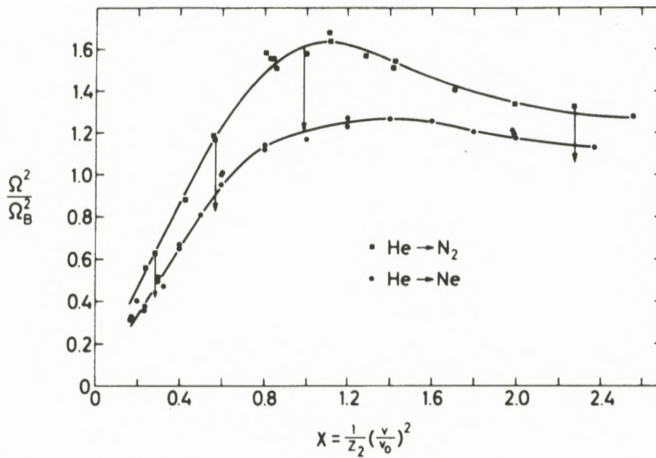
Figure 16. Straggling of helium ions in neon gas and molecular nitrogen. Curves drawn to guide the eye. Upper line: N_2; lower line: Ne. Arrows indicate a theoretical estimate of the correction for molecular correlation. From Besenbacher et al. (1977).
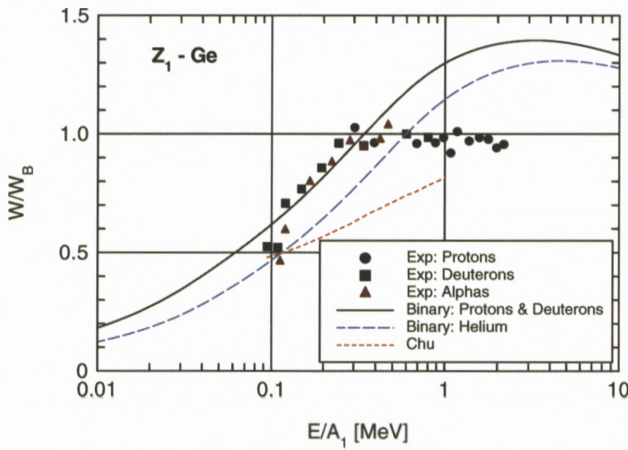
Figure 17. Straggling of light ions in solid germanium. Measurements from Malherbe and Al-bertz (1982). Calculations from binary theory and from Chu (1976). From Sigmund and Schinner (2002a).

Careful straggling measurements on foils with a well-controlled thickness, with ion-target combinations and velocities chosen such as to specifically test the roles of shell and Barkas–Andersen corrections, bunching and correlation, are highly desirable.

3.2. ENERGY-LOSS SPECTRA

According to Bohr (1948), an energy-loss profile approaches Gaussian shape for $\Omega^2 \gg T_{\max}^2$, where $T_{\max}$ is the maximum energy transfer in an individual collision event. For a penetrating point charge this implies

$$4\pi Z_1^2 Z_2 e^4 N x \gg (2mv^2)^2. \tag{9}$$

Evidently, the lower limit in layer thickness for the Gaussian approximation to apply depends most sensitively on Z_1 and on the projectile speed. Specifically, deviations from Gaussian shape are expected to be most pronounced for protons and antiprotons at high speed.

For a detailed discussion, the reader is referred to Sigmund (2006) and a forthcoming paper by Glazov and Sigmund (2006). Here I shall briefly go through the various regimes and the way to treat them theoretically, in the order of increasing thickness:

1. For the thinnest targets, the observed spectrum will resemble the differential scattering cross section and reveal the shell structure of the excitation spectrum of the target. Spectra may be predicted by the convolution method (Bichsel and Saxon, 1975).
2. With increasing layer thickness, shell structure effects will be wiped out, and a more continuous spectrum will emerge which may be approximated by the Landau formula based on Coulomb scattering (Landau, 1944).
3. While the validity of the Landau formula is limited to rather small target thicknesses, an extension of the scheme by Glazov (2000) has proven to be very powerful.
4. The approach to Gaussian shape, which happens to be rather slow, is well described by the method of steepest descent as outlined by Sigmund and Winterbon (1985).
5. As indicated above, Gaussian profiles are more common for $Z_1 \gg 1$, even at high speed, but
6. Non-stochastic broadening may cause deviations from Gaussian shape for large target thicknesses. This effect will occur even in the absence of straggling: Since the initial spectrum always has a non-zero width, the very dependence of the stopping cross section on beam energy will eventually cause the spectrum to broaden in a way that does not preserve an initial Gaussian shape (Payne, 1969).

Figure 18 shows parameters characterizing the energy-loss profile of a point charge according to Glazov (2002a). The abscissa variable $\Omega_{\mathrm{B}}^2 / T_{\max}^2$ represents a
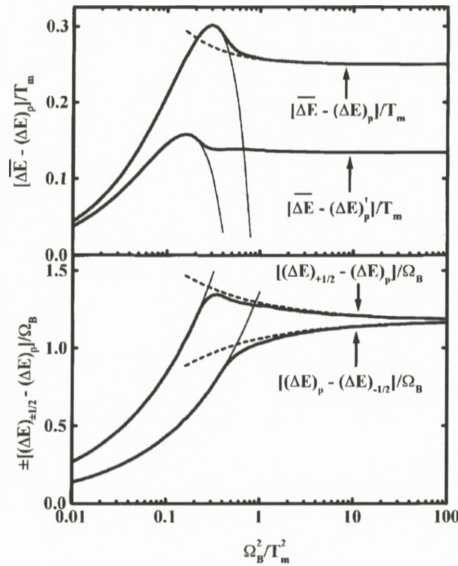
Figure 18. Quantities characteristic of energy-loss spectra calculated for truncated-Coulomb interaction. Thick lines: Numerical from Bothe–Landau equation. Thin lines: Extended Landau approximation due to Glazov (2000). Dotted lines: Steepest-descent method due to Sigmund and Winterbon (1985). $\overline{\Delta E}$ represents the mean energy loss, $(\Delta E)_p$ the peak position, and $(\Delta E)'_p$ the mean value between the left and the right half-value $(\Delta E)_{\pm 1/2}$. From Glazov (2002a).

measure of the target thickness. According to Bohr (1948), the abscissa value 1 represents the dividing point between non-Gaussian and close-to-Gaussian behavior. The upper graph shows the deviation from the peak energy loss ΔE_p from the mean energy loss $\overline{\Delta E}$, as well as the same quantity for a modified peak energy loss $(\Delta E_p)'$, found by taking the average between the upper and lower halfwidth. The difference is striking. The lower graph shows the upper and the lower halfwidth of the projectile. The difference between the two is a measure of the skewness of the profile, which is seen to vanish only at $\Omega^2/T^2_{\max} \geq 100$.

Thick solid lines represent numerical solutions of the Bothe-Landau equation, which comprises the statistical aspects for random stopping under the condition of small total energy loss $\overline{\Delta E} \ll E$. Thin lines represent Glazov's extension of the Landau scheme, while dotted lines represent results of the steepest-descent method. It is seen that combination of the latter two approaches makes up a very satisfactory description, with only a very small error in the immediate vicinity of the cross-over.

Much more drastic deviations from Gaussian shape have been studied extensively in situations where charge exchange plays a significant role. Experimental

studies were performed both for light and heavy ions (Cowern et al., 1984; Ogawa et al., 1991, 1993; Blazevic et al., 2002), and efficient formalisms have been established for theoretical analysis (Winterbon, 1977; Sigmund, 1992; Glazov, 2002b).

4. Low-Velocity Stopping

Some aspects of low-velocity stopping ($v < v_0$) are discussed in the contribution by Arista (2006). In this contribution I shall primarily try to identify needs for information on stopping data for low-speed ions.

4.1. APPLICATION AREAS

With the exception of the lightest ions, nuclear stopping represents the dominating loss mechanism for $v \ll v_0$. This represents a complication with regard to extracting accurate data on electronic stopping from energy-loss measurements (Fastrup et al., 1966). Data on electronic losses are needed primarily for the understanding of radiation effects such as secondary electron emission, particle detectors, and electronic sputtering.

A topic of particular interest is that of elastic-collision spikes (Sigmund, 1974): A spike is a limited volume in a medium exposed to irradiation, where the majority of the atoms is temporarily in motion. Elastic collisions in such a spike lead to redistribution of kinetic energy amongst the atoms, whereas the slowing-down process is very inefficient. Under these circumstances, electronic energy loss may be the main cooling mechanism of a spike, together with energy transport by phonons, even though the electronic stopping cross section may be significantly smaller than the cross section for nuclear stopping which is conventionally determined for a target atom initially at rest.

4.2. STANDARD DESCRIPTIONS

Electronic stopping cross sections have traditionally been evaluated from the Thomas–Fermi models of Lindhard and Scharff (1961) and Firsov (1959). Several attempts have been made to incorporate experimentally observed Z_1 structure into these models, with limited success. For summaries, the reader is referred to Sigmund (2004) or ICRU (2005). More recent work focused almost exclusively on stopping in an electron gas. An early attempt by Finnemann (1968) to describe low-velocity stopping in terms of quantum mechanical phase shifts has proven very successful, both in linear (Briggs and Pathak, 1974) and nonlinear
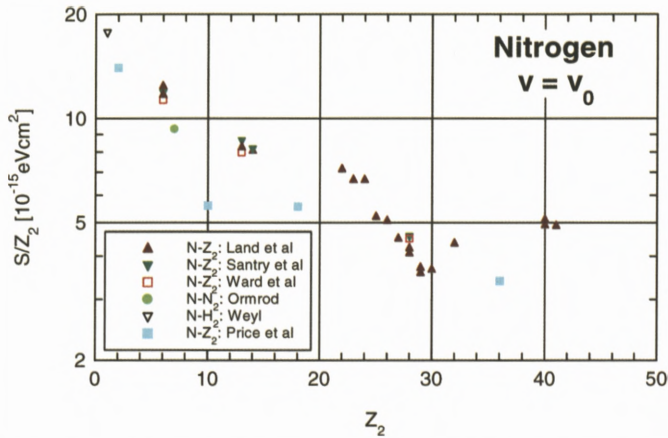
Figure 19. Stopping cross sections for nitrogen ions at $v = v_0$ measured by Land et al. (1985), Santry and Werner (1991), Ward et al. (1979), Ormrod (1968), Weyl (1953) and Price et al. (1993). Data not referring to exactly $v = v_0$ were scaled assuming velocity-proportional stopping. From ICRU (2005).

(Echenique et al., 1981) versions. Interestingly, while relatively weak Z_1 oscillations for random stopping seem to have escaped accurate theoretical description, much more pronounced structure observed in channeling (Bøttiger and Bason, 1969) has received a satisfactory explanation in terms of phase shifts calculated from density functional theory (Ashley et al., 1986) .

4.3. OPEN PROBLEMS

First of all, theory for low-velocity stopping in *insulators* is essentially nonexisting. Existing experience in atomic-collision physics suggests electron promotion to be of prime importance, but even for collisions in the gas phase, valid theoretical predictions seem to address mainly inner-shell phenomena.

Second, the problem of the threshold for electronic energy transfer is essentially unsolved, not only for heavy ions but even for protons and antiprotons, as is manifest in a recent series of publications on stopping in lithium fluoride (Eder et al., 1997; Møller et al., 2002). Experiments indicate, however, that the stopping cross section for protons and antiprotons in LiF is proportional to projectile speed significantly below the binary-collision threshold.

Finally, the suggestion has been made that there is a gas-solid effect in lowvelocity stopping of heavy ions (Paul, 2004). Figure 19 shows measured stopping cross sections from various sources for nitrogen ions at $v = v_0$. Evidently, the noble gases He, Ne, Ar and Kr show lower stopping cross sections than numerous
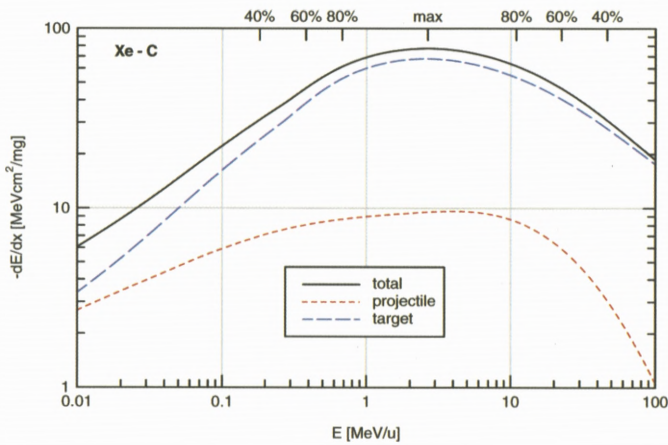
Figure 20. Stopping force of amorphous carbon for xenon ions, calculated from binary theory. Contributions due to target and projectile excitations are shown separately, as well as their sum.

other elements. However, it is not clear whether this is an effect of Z_2 structure or a gas-solid effect. Note in particular that nitrogen gas – according to a different source – shows a much less pronounced effect.

5. Velocity Effect for Swift Ions

Several contributions to this volume mention the so-called velocity effect, i.e., the experimental finding that radiation effects originating in electronic energy loss do not necessarily scale with the stopping cross section. A common feature for such phenomena is the double-valuedness of the physical quantity of interest, such as a sputter yield of a solid or an inactivation rate of a cell culture, when plotted as a function of the stopping cross section.

Clearly, the differential energy-transfer cross section at two different values of the beam energy will not be the same, even if the stopping cross sections happen to coincide. But how large is the difference, and in which part of the excitation spectrum is it most pronounced?

Figure 20 shows the calculated equilibrium stopping force on xenon in carbon. Contributions from target and projectile excitation are shown separately. The upper abscissa scale shows the position of the maximum as well as the 80, 60 and 40% levels below the maximum.

Figure 21 shows single-differential cross sections for electron emission – i.e. integrated over emission angle – for target excitation/ionization and the whole spectrum, respectively. Cross sections were calculated from the PASS code ac-
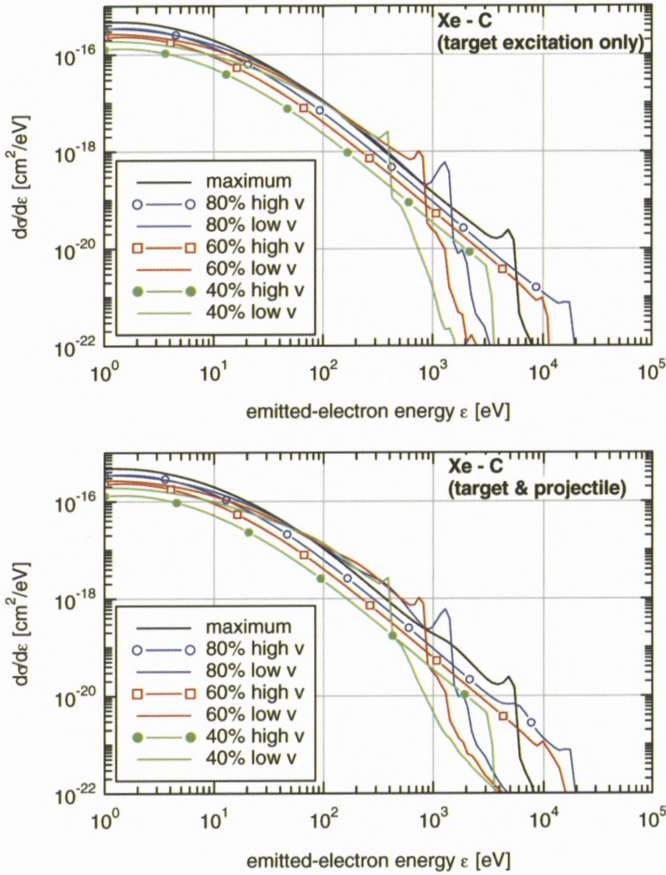
Figure 21. Energy spectra of electrons emitted in a single Xe-C collision. Beam energies chosen at maximum stopping as well as the 80, 60 and 40% level indicated in figure 20. Upper graph: Target excitation only. Lower graph: Total spectrum.

cording to a theoretical scheme described by Weng et al. (2006). Spectra for the various levels are distinguished by their colors.

As expected, the spectrum reflecting the higher beam energy extends to a higher electron energy ϵ than that for the lower beam energy. That difference, however, is compensated by a pronounced shoulder of the low-energy spectrum near its kinematic limit. Conversely, only minor differences are observed at the low-energy end of the spectra, despite a factor of 10–100 difference between the respective beam energies. Note that from Rutherford's law – which is the standard theoretical tool in this kind of analysis (Kobetich and Katz, 1968; Wilson and

Paretzke, 1981; Scholz and Kraft, 1995) one would expect a difference in the two spectra at the lower end of one to two orders of magnitude!

6. Conclusions

Although I have not dwelled on this aspect, I like to emphasize that classical mechanics is a powerful tool in the description of electronic stopping and related problems. This has proven particularly true for ions heavier than helium, but even in the velocity range that is commonly identified as the Born regime, not much more quantum physics is needed to achieve a valid description than what is contained in the Bloch correction, which does not contain target parameters.

Amongst longstanding problems which may be considered "solved" at least in principle, I like to mention

- the gas-solid effect in the stopping force on heavy ions, except at low speed,
- the (lacking) role of the effective charge in heavy-ion stopping,
- the magnitude of the Barkas–Andersen effect in close collisions,
- the physics of the shell correction, and
- deviations from Bragg additivity and other valence effects.
- Efficient tools are available to analyse the role of charge exchange in straggling, but the potential of utilizing information from pertinent experiments has not been fully utilized yet.

Amongst aspects that I believe need adequate attention I should like to mention

- careful distinction between energy loss and deposition,
- low-velocity stopping in insulators,
- the role of electron promotion in stopping and straggling,
- clear criteria for the significance of charge exchange in stopping,
- the Barkas–Andersen effect in channeling,
- the gas-solid effect in straggling,
- the role of bunching and correlation in straggling, mostly in solids, and the competition with the Bethe–Livingston shoulder.

Acknowledgements

References

Ahlen S.P. (1980): Theoretical and experimental aspects of the energy loss of relativistic heavily ionizing particles. Rev Mod Phys **52**, 121–173

Ahlen S.P. (1982): Calculation of the relativistic Bloch correction to stopping power. Phys Rev A **25**, 1856–1867

Andersen H.H., Garfinkel A.F., Hanke C.C. and Sørensen H. (1966): Stopping power of aluminium for 5-12 MeV protons and deuterons. Mat Fys Medd Dan Vid Selsk **35, no. 4**, 1–24

Andersen H.H., Simonsen H. and Sørensen H. (1969a): An experimental investigation of charge-dependent deviations from the Bethe stopping power formula. Nucl Phys A **125**, 171–175

Andersen H.H., Sørensen H. and Vajda P. (1969b): Excitation potentials and shell corrections for elements $Z_2 = 20$ to $Z_2 = 30$. Phys Rev **180**, 373–380

Arista N.R. (2002): Energy loss of heavy ions in solids: -linear calculations for slow and swift ions. Nucl Instrum Methods B **195**, 91–105

Arista N.R. (2006): Charge states and energy loss of ions in solids. Mat Fys Medd Dan Vid Selsk **52**, 595–623

Ashley J.C., Ritchie R.H. and Brandt W. (1972): Z_1^3 Effect in the stopping power of matter for charged particles. Phys Rev B **5**, 2393–2397

Ashley J.C., Ritchie R.H., Echenique P.M. and Nieminen R.M. (1986): Nonlinear calculations of the energy loss of slow ions in an electron gas. Nucl Instrum Methods B **15**, 11–13

Azevedo G.M., Grande P.L., Behar M., Dias J.F. and Schiwietz G. (2001): Giant Barkas effect observed for light ion channeling in Si. Phys Rev Lett **86**, 1482–1485

Azevedo G.M., Grande P.L. and Schiwietz G. (2000): Impact-parameter dependent energy loss of screened ions. Nucl Instrum Methods B **164-165**, 203–211

Besenbacher F., Andersen J.U. and Bonderup E. (1980): Straggling in energy loss of energetic hydrogen and helium ions. Nucl Instrum Methods **168**, 1–15

Besenbacher F., Andersen H.H., Hvelplund P. and Knudsen H. (1981): Straggling in energy loss of swift hydrogen and helium ions in gases. Mat Fys Medd Dan Vid Selsk **40, no. 9**, 1–42

Besenbacher F., Heinemeier J., Hvelplund P. and Knudsen H. (1977): Energy-loss straggling for protons and helium ions. Phys Lett A **61**, 75–77

Betz H.D. and Grodzins L. (1970): Charge states and excitation of fast heavy ions passing through solids: a new model for the density effect. Phys Rev Lett **25**, 211–214

Bichsel H. and Saxon R.P. (1975): Comparison of calculational methods for straggling in thin absorbers. Phys Rev A **11**, 1286–1296

Bimbot R., Cabot C., Gardès D., Gauvin H., Hingmann R., Orliange I., De Reilhac L. and Hubert F. (1989a): Stopping power of gases for heavy ions: as-solid effect I. 2-13 MeV/u Ne and Ar projectiles. Nucl Instrum Methods B **44**, 1–18

Bimbot R., Cabot C., Gardès D., Gauvin H., Orliange I., DeReilhac L., Subotic K. and Hubert F. (1989b): Stopping power of gases for heavy ions: gas-solid effect II. 2-6MeV/u Cu, Kr and Ag projectiles. Nucl Instrum Methods B **44**, 19–34

Blazevic A., Bohlen H.G. and von Oertzen W. (2002): Stopping power of swift neon ions in dependence on the charge state in the non-equilibrium regime. Nucl Instrum Methods B **190**, 64–68

Bloch F. (1933): Zur Bremsung rasch bewegter Teilchen beim Durchgang durch Materie. Ann Physik **16**, 285–320

Bohr N. (1940): Scattering and stopping of fission fragments. Phys Rev **58**, 654–655

Bohr N. (1948): The penetration of atomic particles through matter. Mat Fys Medd Dan Vid Selsk **18, no. 8**, 1–144

Bohr N. and Lindhard J. (1954): Electron capture and loss by heavy ions penetrating through matter. Mat Fys Medd Dan Vid Selsk **28, no. 7**, 1–31

Bonderup E. (1967): Stopping of swift protons evaluated from statistical atomic model. Mat Fys Medd Dan Vid Selsk **35, no. 17**, 1–20

Bonderup E. and Hvelplund P. (1971): Stopping power and energy straggling for swift protons. Phys Rev A **4**, 562–589

Bøttiger J. and Bason F. (1969): Energy loss of heavy ions along low-index directions in gold single crystals. Radiat Eff **2**, 105

Briggs J.S. and Pathak A.P. (1974): The stopping power of solids for low-velocity channelled heavy ions. J Phys C **7**, 1929–1936

Cabrera-Trujillo R., Sabin J.R., Deumens E. and Öhrn Y. (2002): Stopping cross sections for $N^{4+} \rightarrow H$ at low velocity. Phys Rev A **66**, 022706, 1–7

Chu W.K. (1976): Calculation of energy straggling for protons and helium ions. Phys Rev A **13**, 2057–2060

Chu W.K. and Powers D. (1972): Calculations of mean excitation energy for all elements. Phys Lett **40A**, 23–24

Cowern N.E.B., Read P.M., Sofield C.J., Bridwell L.B. and Lucas M.W. (1984): Charge-changing energy loss, higher-order Z_1 dependence, and pre-equilibrium behavior in the stopping power for energetic ions in solids. Phys Rev A **30**, 1682–1691

Datz S., DelCampo J.G., Dittner P.F., Miller P.D. and Biggerstaff J.A. (1977): Higher-order Z_1 effects and effects of screening by bound K electrons on the electronic stopping of channeled ions. Phys Rev Lett **38**, 1145–1148

Dehmer J.L., Inokuti M. and Saxon R.P. (1975): Systematics of dipole oscillator-strength distributions for atoms of the first and second row. Phys Rev A **12**, 102–121

Echenique P.M., Nieminen R.M. and Ritchie R.H. (1981): Density functional calculation of stopping power of an electron gas for slow ions. Sol St Comm **37**, 779–781

Eder K., Semrad D., Bauer P., Golser R., Maier-Komor P., Aumayr F., Peñalba M., Arnau A., Ugalde J.M. and Echenique P.M. (1997): Absence of a "threshold effect" in the energy loss of slow protons traversing large-band-gap insulators. Phys Rev Lett **79**, 4112–4115

Fano U. (1963): Penetration of protons, alpha particles, and mesons. Ann Rev Nucl Sci **13**, 1–66

Fastrup B., Hvelplund P. and Sautter C.A. (1966): Stopping cross section in carbon of 0.1–1.0 MeV atoms with $6 < Z_1 < 20$. Mat Fys Medd Dan Vid Selsk **35, no. 10**, 1–28

Finnemann J. (1968): En redegørelse for resultaterne af beregninger over spredning af elektroner med lav energi på afskærmede Coulombfelter. Master's thesis, Aarhus University

Firsov O.B. (1959): A qualitative interpretation of the mean electron excitation energy in atomic collsions. Zh Eksp Teor Fiz **36**, 1517–1523. [English translation: Sov. Phys. JETP **9**, 1076-1080 (1959)]

Geissel H. (1982): Untersuchungen zur Abbremsung von Schwerionen in Materie im Energiebereich von (0,5–10) MeV/U. GSI-Report **82-12**, 21–29

Glazov L.G. (2000): Energy-loss spectra of swift ions. Nucl Instrum Methods B **161**, 1–8

Glazov L.G. (2002a): Energy-loss spectra of swift ions: Beyond the Landau approximation. Nucl Instrum Methods B **192**, 239–248

Glazov L.G. (2002b): Multiple-peak structures in energy-loss spectra of swift ions. Nucl Instrum Methods B **193**, 56–65

Glazov L.G. and Sigmund P. (2006): Energy-loss spectra of swift point charges at relativistic velocities. Nucl Instrum Methods B, in press

Golovchenko J.A., Goland A.N., Rosner J.S., Thorn C.E., Wegner H.E., Knudsen H. and Moak C.D. (1981): Charge state dependence of channeled ion energy loss. Phys Rev B **23**, 957–966

Golser R. and Semrad D. (1991): Observation of a striking departure from velocity proportionality in low-energy electronic stopping. Phys Rev Lett **66**, 1831–1833

Grande P.L. and Schiwietz G. (2002): The unitary convolution approximation for heavy ions. Nucl Instrum Methods B **195**, 55–63

Grande P.L., Hentz A., Pezzi R.P., Baumvoll I.J.R. and Schiwietz G. (2006): Solved and unsolved problems in ion-beam analysis: The influence of single collisions. Mat Fys Medd Dan Vid Selsk **52**, 151–185

Grüner F., Bell F., Assmann W. and Schubert M. (2004): Integrated approach to the electronic interaction of swift heavy ions with solids and gases. Phys Rev Lett **93**, 213201

Henke B.L., Gullikson E.M. and Davies J.C. (1993): X-ray interactions: photoabsorption, scattering, transmission, and reflection at E = 50-30,000 eV, Z = 1-92. At Data & Nucl Data Tab **54**, 181–342

Holmén G., Svensson B.G., Schou J. and Sigmund P. (1979): Direct and recoil-induced electron emission from ion-bombarded solids. Phys Rev B **20**, 2247–2254

ICRU (1993): Stopping Powers and Ranges for Protons and Alpha Particles, Vol. 49 of ICRU Report. International Commission of Radiation Units and Measurements, Bethesda, Maryland

ICRU (2005): Stopping of Ions Heavier Than Helium, Vol. 73 of ICRU Report. Oxford University Press, Oxford

Jäkel O. (2006): Hadron therapy: Radiotherapy using fast ion beams. Mat Fys Medd Dan Vid Selsk **52**, 37–57

Kabachnik N.M. (1993): Screening and antiscreening in the semiclassical description of ionization in fast ion-atom collisions. J Phys B **26**, 3803–3814

Kobetich E.J. and Katz R. (1968): Energy deposition by electron beams and delta rays. Phys Rev **170**, 391–396

Land D.J., Simons D.G., Brennan J.G. and Glass G.A. (1985): Range distributions and electronic stopping power of nitrogen ions in solids. Nucl Instrum Methods B **10/11**, 234–236

Landau L. (1944): On the energy loss of fast particles by ionization. J Phys USSR **8**, 201–205

Lassen N.O. (1951a): Total charges of fission fragments as functions of the pressure in the stopping gas. Mat Fys Medd Dan Vid Selsk **26, no. 12**, 1–19

Lassen N.O. (1951b): The total charges of fission fragments in gaseous and solidstopping media. Mat Fys Medd Dan Vid Selsk **26, no. 5**, 1–28

Lindhard J. (1965): Influence of crystal lattice on motion of energetic charged particles. Mat Fys Medd Dan Vid Selsk **34, no. 14**, 1–64

Lindhard J. (1976): The Barkas effect – or Z_1^3, Z_1^4-corrections to stopping of swift charged particles. Nucl Instrum Methods **132**, 1–5

Lindhard J. and Scharff M. (1953): Energy loss in matter by fast particles of low charge. Mat Fys Medd Dan Vid Selsk **27, no. 15**, 1–31

Lindhard J. and Scharff M. (1961): Energy dissipation by ions in the keV region. Phys Rev **124**, 128–130

Lindhard J. and Sørensen A.H. (1996): On the relativistic theory of stopping of heavy ions. Phys Rev A **53**, 2443–2456

Malherbe J.B. and Albertz H.W. (1982): Energy-loss straggling in C and Ge of p, D and alpha particles in the energy region 0.2 to 2.4 MeV. Nucl Instrum Methods **192**, 559–563

Maynard G., Chabot M. and Gardès D. (2000): Density effect and charge dependent stopping theories for heavy ions in the intermediate velocity regime. Nucl Instrum Methods B **164-165**, 139–146

Maynard G., Zwicknagel G., Deutsch C. and Katsonis K. (2001): Diffusion-transport cross section and stopping power of swift heavy ions. Phys Rev A **63**, 052903-1–14

Medenwaldt R., Møller S.P., Uggerhøj E., Worm T., Hvelplund P., Knudsen H., Elsener K. and Morenzoni E. (1991): Measurement of the stopping power of silicon for antiprotons between 0.2 and 3 MeV. Nucl Instrum Methods B **58**, 1–5

Meitner L. and Freitag K. (1926): Über die Alpha-Strahlen des ThC+C' und ihr Verhalten beim Durchgang durch verschiedene Gase. Z Physik **37**, 481–517

Mikkelsen H.H. and Mortensen E.H. (1990): The extended oscillator model of atomic stopping - application to proton stopping in noble gases. Nucl Instrum Methods B **48**, 39–42

Mikkelsen H.H. and Sigmund P. (1987): Impact parameter dependence of electronic energy loss: Oscillator model. Nucl Instrum Methods B **27**, 266–275

Mikkelsen H.H. and Sigmund P. (1989): Barkas effect in electronic stopping power: Rigorous evaluation for the harmonic oscillator. Phys Rev A **40**, 101–116

Møller S.P., Uggerhøj E., Bluhme H., Knudsen H., Mikkelsen U., Paludan K. and Morenzoni E. (1997): Direct measurement of the stopping power for antiprotons of light and heavy targets. Phys Rev A **56**, 2930–2939

Møller S.P., Csete A., Ichioka T., Knudsen H., Uggerhoj U.I. and Andersen H.H. (2002): Antiproton stopping at low energies: confirmation of velocity-proportional stopping power. Phys Rev Lett **88**, 193201-1–4

Montanari C.C., Miraglia J.E. and Arista N.R. (2003): Antiscreening mode of projectile-electron loss. Phys Rev A **67**, 062702

Northcliffe L.C. (1963): Passage of heavy ions through matter. Ann Rev Nucl Sci **13**, 67–102

Oddershede J. and Sabin J.R. (1984): Orbital and whole-atom proton stopping power and shell corrections for atoms with $Z < 36$. At Data Nucl Data Tab **31**, 275–297

Ogawa H., Katayama I., Ikegami H., Haruyama Y., Aoki A., Tosaki M., Fukuzawa F., Yoshida K., Sugai I. and Kaneko T. (1991): Direct Measurement of fixed-charge stopping power for 32-MeV He^{3+} in a charge-state nonequilibrium region. Phys Rev B **43**, 11370–11376

Ogawa H., Katayama I., Sugai I., Haruyama Y., Saito M., Yoshida K., Tosaki M. and Ikegami H. (1993): Charge state dependent energy loss of high velocity oxygen ions in the charge state non-equilibrium region. Nucl Instrum Methods B **82**, 80–84

Ormrod J.H. (1968): Low-energy electronic stopping cross sections in nitrogen and argon. Can J
    Phys **46**, 497–502

Palik E.D. (2000): Electronic Handbook of Optical Constants of Solids – Version 1.0. SciVision –
    Academic Press

Paul H. (2004): A note on the density effect in the stopping power for positive ions. Nucl Instrum
    Methods B **217**, 7–11

Paul H. (2005): Stopping power graphs. `www.exphys.uni-linz.ac.at/stopping/`

Payne M.G. (1969): Energy straggling of heavy charged particles in thick absorbers. Phys Rev **185**,
    611–622

Price J.L., Simons D.G., Stern S.H., Land D.J., Guardala N.A., Brennan J.G. and Stumborg M.F.
    (1993): Stopping powers of the noble gases for (0.3-10)-MeV nitrogen ions. Phys Rev A **47**,
    2913–2918

Santry D. and Werner R. (1991): Measured stopping powers of ^{12}C and ^{14}N ions in thin elemental
    foils. Nucl Instrum Methods B **53**, 7–14

Scheidenberger C., Geissel H., Mikkelsen H.H., Nickel F., Brohm T., Folger H., Irnich H., Magel
    A., Mohar M.F., Pfützner G.M.M. et al. (1994): Direct observation of systematic deviations
    from the Bethe stopping theory for relativistic heavy ions. Phys Rev Lett **73**, 50–53

Schiøtt H.E. (1966): Range-energy relations for low-energy ions. Mat Fys Medd Dan Vid Selsk **35,
    no. 9**, 1

Schiwietz G. (1990): Coupled-channel calculation of stopping powers for intermediate-energy light
    ions penetrating atomic H and He targets. Phys Rev A **42**, 296–306

Scholz M. and Kraft G. (1995): Track structure and the calculation of biological effects of heavy
    charged particles. Adv Space Res **18**, 5–14

Sigmund P. (1974): Energy density and time constant of heavy-ion-induced elastic-collision spikes
    in solids. Appl Phys Lett **25**, 169–171

Sigmund P. (1976): Energy loss of charged particles to molecular gas targets. Phys Rev A **14**,
    996–1005

Sigmund P. (1978): Statistics of particle penetration. Mat Fys Medd Dan Vid Selsk **40, no. 5**, 1–36

Sigmund P. (1982): Kinetic theory of particle stopping in a medium with internal motion. Phys Rev
    A **26**, 2497–2517

Sigmund P. (1992): Statistical theory of charged-particle stopping and straggling in the presence of
    charge exchange. Nucl Instrum Methods B **69**, 113–122

Sigmund P. (1996): Low-velocity limit of Bohr's stopping-power formula. Phys Rev A **54**, 3113–
    3117

Sigmund P. (1997): Charge-dependent electronic stopping of swift nonrelativistic heavy ions. Phys
    Rev A **56**, 3781–3793

Sigmund P. (2004): Stopping of Heavy Ions, Springer Tracts of Modern Physics, Vol. 204. Springer,
    Berlin

Sigmund P. (2006): Particle Penetration and Radiation Effects, Springer Series in Solid-State
    Sciences, Vol. 151. Springer, Berlin

Sigmund P. and Glazov L.G. (2003): Interplay of charge exchange and projectile excitation in the
    stopping of swift heavy ions. Europ Phys J D **23**, 211–215

Sigmund P. and Haagerup U. (1986): Bethe stopping theory for a harmonic oscillator and Bohr's
    oscillator model of atomic stopping. Phys Rev A **34**, 892–910

Sigmund P. and Schinner A. (2000): Binary stopping theory for swift heavy ions. Europ Phys J D
    12, 425–434

Sigmund P. and Schinner A. (2001a): Effective charge and related/unrelated quantities in heavy-ion stopping. Nucl Instrum Methods B **174**, 535–540

Sigmund P. and Schinner A. (2001b): Resolution of the frozen-charge paradox in stopping of channeled heavy ions. Phys Rev Lett **86**, 1486–1489

Sigmund P. and Schinner A. (2002a): Barkas effect, shell correction, screening and correlation in collisional energy-loss straggling of an ion beam. Europ Phys J D 201–209

Sigmund P. and Schinner A. (2002b): Binary theory of electronic stopping. Nucl Instrum Methods B **195**, 64–90

Sigmund P. and Schinner A. (2003): Anatomy of the Barkas effect. Nucl Instrum Methods B **212**, 110 – 117

Sigmund P. and Schinner A. (2006): Shell correction in stopping theory. Nucl Instrum Methods B **243**, 457–460

Sigmund P. and Winterbon K.B. (1985): Energy loss spectrum of swift charged particles penetrating a layer of material. Nucl Instrum Methods B **12**, 1–16

Sigmund P., Fettouhi A. and Schinner A. (2003): Material dependence of electronic stopping. Nucl Instrum Methods B **209**, 19–25

Sigmund P., Sharma A., Schinner A. and Fettouhi A. (2005): Valence structure effects in the stopping of swift ions. Nucl Instrum Methods B **230**, 1–6

Tarlé G. and Solarz M. (1978): Evidence for higher-order contributions to the stopping power of relativistic iron nuclei. Phys Rev Lett **41**, 483–486

Thwaites D.I. (1984): Current status of physical state effects on stopping power. Nucl Instrum Methods B **12**, 84–89

Walske M.C. (1952): The stopping power of K-electrons. Phys Rev **88**, 1283–1289

Ward D., Andrews H.R., Mitchell I.V., Lennard W.N., Walker R.B. and Rud N. (1979): Systematics for the Z_1-oscillation in stopping powers of various solid materials. Can J Phys **57**, 645–656

Weng M.S., Schinner A., Sharma A. and Sigmund P. (2006): Primary electron spectra from swift heavy-ion impact: Scaling relations and estimates from modified Bohr theory. Europ Phys J D **39**, 209–221

Weyl P.K. (1953): The energy loss of hydrogen, helium, nitrogen, and neon ions in gases. Phys Rev **91**, 289–296

Wilson W.E. and Paretzke H.G. (1981): Calculation of distributions for energy imparted and ionization by fast protons in nanometer sites. Radiat Res **87**, 521–537

Winter HP., Aumayr F., Winter H. and Lederer S. (2006): Recent advances in slow heavy particle induced electron emission. Mat Fys Medd Dan Vid Selsk **52**, 525–556

Winterbon K.B. (1977): Electronic energy loss and charge-state fluctuations of swift ions. Nucl Instrum Methods **144**, 311–315

Ziegler J.F. (2005): Particle interactions with matter. www.srim.org